Photon migration in layered media

Ralph Nossal, J. Kiefer, G. H. Weiss, R. Bonner, H. Taitelbaum, and S. Havlin

Surface emission profiles and related functions are computed for particles (photons) migrating within a semi-infinite medium containing a surface layer whose absorbance differs from that of the underlying layer. Photons are assumed to be inserted at a single point on the surface. In certain cases distinct features appear in the emission profiles which enable determination of the thickness of the top layer and of the absorption coefficients of both layers. Computations are performed to provide estimates of parameter ranges for which the presence of one layer distorts photon emission profiles from the other. Several ancillary functions are calculated, including the absorbance profile as a function of depth, the expected path length of photons that are reemitted at a distance ρ from the point of insertion, and the average depth probed by those reemitted photons.

I. Introduction

Many therapeutic and diagnostic techniques in medicine depend on specific local interactions of light with tissue and other biological media. In several applications radiation is incident at the surface of a tissue, and the reemission of photons from that surface provides information about the medium. We, therefore, recently developed a mathematical model to describe photon migration in turbid media.[1] Formulas were obtained for the spatial intensity distribution of diffuse emission at the surface and for the mean total path length traveled by a photon between the point of incidence and the point of reemission. We also were able to find the probability density for photon absorption as a function of depth in the tissue and the average depth at which a photon travels before reemission. These all are useful for interpreting data acquired by remote optical sensing of biological tissue, an example of which is laser Doppler velocimetry to measure microvascular blood flow.[2,3]

As light penetrates biological tissue, it is scattered by many refractive-index variations, which, over distances of the order of 1 mm, lead to the randomization of the direction of propagation. The great variability in microscopic refractive index within the medium makes it almost impossible to analyze scattering in detail for living tissues. However, the specifics of the short range behavior by which light is partially scattered from its initial direction do not need to be understood to describe light propagation over distances substantially greater than that required for the randomization of the direction of propagation. Thus we previously adapted a discrete lattice model as a convenience in carrying out both analytic and numerical calculations. The use of such a lattice random walk should be regarded as a phenomenological approach, justified by comparison to calculations for more physically realistic models, such as in Ref. 1 for a semi-infinite continuum model having random scattering lengths. The continuum model corresponds to a lattice with vanishingly small lattice spacing where randomization of direction occurs over distances which are exponentially distributed about a constant mean value. Such lattice models underly the development of many theories of diffusive motion.[4]

In our earlier work,[1] the homogeneous tissue was assumed to be so thick that only a single surface—the interface between the tissue and the exterior medium—needs be taken into account. In the present work we use the lattice model to examine the effects of tissue heterogeneity by including an additional superficial tissue layer whose absorptive properties differ from those in the underlying bulk medium. Examples of layered biological tissues are skin (epidermis, dermis, subcutaneous fat) and the walls of arteries (intima, muscle, adventitia), stomach, bladder, intestine, and esophagus. Also, different tissues in contact, or tumors within a single tissue, in certain cases might be modeled as being such layers. Two potential clinical applications involve tumor detection and therapy: (1) to detect a deep-lying tumor by examining diffuse

H. Taitelbaum and S. Havlin are with Bar-Ilan University, Physics Department, Ramat-Gan, Israel; the other authors are with National Institute of Health, Bethesda, Maryland 20892; R. Bonner is in the Biomedical Engineering Branch, Division of Research Services, and the other authors are in the Physical Sciences Laboratory, Division of Computer Research & Technology.

Received 14 September 1987.

surface emissions,[5] it is necessary to know how the emitted image is distorted by the intervening tissue, e.g., how thin the upper layer has to be to detect the underlying abnormality; (2) when irradiating pigmented epithelia of finite thickness, such as a region of malignant melanoma tissue in which one is trying to apply phototherapy,[6] one needs to know the depth distribution of light absorption and how the underlying tissue layer affects the absorption profile. A third example derives from attempts to destroy atherosclerotic plaque using laser angioplasty[7]: A scheme by which plaque can be identified optically, and its thickness quantified by remote sensing, might be used to control therapeutic laser ablation. Because in these cases one cannot readily make measurements within the tissues, information may only be available from photons that penetrate and subsequently are reemitted from the surface.

Although Monte Carlo calculations can be carried out for heterogeneous tissue geometries, such simulations are almost useless for examining the characteristics of photon reemission at distances far from the point of insertion because long migration paths occur with low probability. Hence we devised an iterative computational scheme for the lattice occupancy probabilities of migrating particles. This methodology is described in the next section (Sec. II). It is particularly useful when the scattering cross sections (i.e., the scattering lengths) of the various regions of the composite material are similar but when the regions have different average absorptions. For illustration, we specifically consider a two-region composite with a surface layer lying on top of a semi-infinite substrate.

Results from these calculations are presented in Sec. III. First we consider a case where the absorbances of the two layers differ by a factor of 20. Because of this disparity, the effects of the more highly absorbing layer are distinct, and results are easily interpretable (see Figs. 2–9). Insights gained from these studies then facilitate an understanding of the results of corresponding computations performed for layered media in which the absorptive properties are similar (e.g., Figs. 10 and 11).

At this stage of the investigation our principal goal is to provide general qualitative insights into the behavior of photons migrating in layered media rather than to obtain precise numerical results. In Sec. IV we briefly discuss other calculations that are possible using the present methods. The present numerical investigations suggest that it is feasible to estimate useful physical parameters for a two-layered medium from experimental data, especially if the absorbances are dissimilar.

II. Computational Methodology

We wish to simulate the history of a photon after it is injected into a semi-infinite two-layered medium. The kinetics of photon migration are modeled in terms of a random walk on a discrete lattice. However, instead of simulating many random walks and calculating averaged quantities from them, we are able to calculate exact probabilities. The scheme for doing this has been used recently in a number of physical applications.[8,9] Specifically, we assume that a walker starts at radius $r = 0$ and depth $z = 1$ (see Fig. 1). After n steps each site contains a fractional number of walkers corresponding to the probability that a single walker, starting from (0,0,1), will be at that site. Any random walker reaching the surface is considered to be absorbed there and is so recorded.

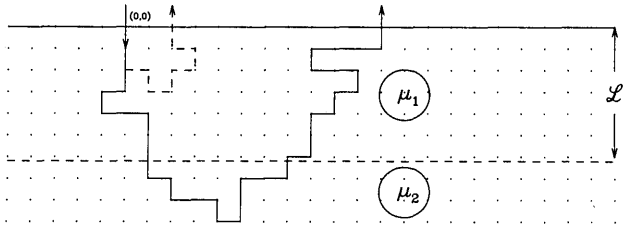

Fig. 1. Two-dimensional projection of semi-infinite layered medium, approximated by a lattice of discrete scattering loci surrounded by continuously absorbing material. The scattering length here is understood to be identical in the two regions, and the absorption coefficients in the top and the bottom layers are μ_1 and μ_2.

In the present work the scattering is presumed to be angularly isotropic. Thus, if we were to use ordinary rectangular coordinates, the probability of moving would be equal to one-sixth in each of the six possible directions. To simplify the computations, we utilize the circular symmetry and divide the migration space into concentric annuli, or rings, whose inner and outer radii are given by $j \pm \frac{1}{2}$ ($j = 1,2,\ldots$). In this case the probability of moving in either direction along the z axis still is one-sixth, but different probabilities are used to describe lateral movements. For a walker in the central core (inner radius = 0, outer radius = $\frac{1}{2}$), the probability of a move outward to the annulus whose ring index is $r = 1$ is two-thirds. However, for a walker in a ring of index $r > 0$, the probability of moving inward is $(\frac{1}{6})[1 - 1/(2r)]$, while the probability of moving outward is $(\frac{1}{6})[1 + 1/(2r)]$. Furthermore, in all cases except the central core, the probability of staying in the same annulus and moving around it one step clockwise or counterclockwise, without changing depth or radius, is one-third. We verify these formulas by the following observations: (1) If the circular shells are replaced by nested squares or hexagons, the probabilities of migration, within a given shell or to its neighbors, also are given by these formulas. (2) If infinite space is uniformly populated by photons, migration according to these formulas keeps the distribution uniform.

One complication is that at each step some of the walkers are absorbed. Absorption is assumed to be described by Beer's law, i.e., $\exp(-\mu)$ is the survival probability per unit step, where μ is the absorption coefficient per unit scattering length.[1] By convention, we assume that, at the interface between the two tissue phases, the material of the upper layer extends to a depth of $\mathcal{L} + \epsilon$, where ϵ is a vanishingly small quantity.

Thus, when scattering occurs toward the surface or in the plane defined by $z = \mathcal{L}$, the subpopulation of random walkers is decreased by a term depending on the absorption of the upper region; when scattering at the $\mathcal{L}$th layer is directed downward into the material, the absorbed fraction is given by the properties of the lower region.

In our numerical work, the lattice typically contains $z_m = 130$ total depth levels and $r_m = 130$ concentric rings. To obtain the number of walkers that decay at each of the i levels, we count the total number of walkers at depth i and multiply by the fraction $[1 - \exp(-\mu_i)]$, where μ_i is the absorption coefficient per unit scattering length at the ith level. {In accordance with our convention, at the interface $z = \mathcal{L}$ we multiply by $[1 - (\frac{5}{6}) \exp(-\mu_{\text{upper}}) - (\frac{1}{6}) \exp(-\mu_{\text{lower}})]$.} Then, beginning at the center, we process each ring successively. The use of two grids, old walker and new walker, facilitates the procedure of dividing and allocating probability densities. We count and remove the walkers that reach the remote surfaces of our large but finite array, asserting that only a fraction of the walkers impinging on the fictitious boundary is absorbed. (We arbitrarily take that fraction to be one-half but find that the particular choice does not significantly affect results.) Next, for each ring, we compute the cumulative number of walkers that have surfaced, both unweighted and weighted by step number. At the end of the simulation the unweighted number is used to determine the photon emission profile. The step-weighted quantity is used to calculate the average path length (step number) of those photons that surface within any given ring. All calculations are repeated until the number of active walkers (those which neither leaked at the boundaries nor were absorbed within the medium) falls below a preset value (typically 10^{-10}, which corresponds to ~1000–2000 iterative steps).

An additional parameter of physical interest is the average depth of a photon that emerges at a distance ρ from the injection point. An adaptation of the exact enumeration method, utilizing two registers at each site, is used to calculate this quantity.

III. Results

A. Disparate Absorption

We begin by examining cases in which the absorption coefficients of the two layers are very different. Insights gained from this part of the investigation facilitate later interpretation of calculations for photon migration in layered media having similar absorption coefficients.

Measurable quantities in the anticipated applications consist of surface emission data obtained at various distances ρ from the entrance point of the laser beam. However, because the numerical simulations are performed for a lattice model, results will be given in terms of the function G_r, defined to be the fraction of photons reemitted within the rth annulus on the surface. These data can be related to the function $\gamma(\rho)$, defined as the probability density that a photon exits the medium at distance ρ; i.e., $\gamma(\rho)d\rho$ is the reemitted radiation at a distance lying between ρ and $\rho + d\rho$ [see Eq. (11) of Ref. 1].

1. *Form of the Surface Emission Profile*

First we consider the case where absorption within the surface layer is very much greater than that within the lower region ($\mu_1 \gg \mu_2$). In Fig. 2(a) we show surface profiles G_r for $\mu_1 = 0.2$, $\mu_2 = 0.01$, computed for differing values of the thickness $\mathcal{L}$ (in lattice units) of the upper layer, where the quantities μ_1 and μ_2 are the absorption coefficients of the upper and lower layers, respectively. It has been shown in Ref. 1 [from Eqs. (12) and (14)] that the function $\gamma(\rho)$ for a homogeneous medium is

$$\gamma(\rho) \sim \rho^{-1} \exp[-\rho(6\mu)^{1/2}], \tag{1}$$

for sufficiently large ρ. Thus, when the bottom layer has the same absorption coefficient as does the top, we expect the quantity $\log(rG_r)$ to vary as a straight line with the slope given as $-(6\mu_1)^{1/2}$. This is demonstrated in Fig. 2(b), where the results shown in Fig. 2(a) are replotted as rG_r on semilogarithmic axes. The slope of the line marked ∞, which corresponds to a homogeneous material, indeed has the expected behavior. More interesting, however, is the fact that for large r the slopes of the other lines on the graph are given as $d[\log(rG_r)]/dr = -(6\mu_2)^{1/2}$. Thus, in principle, the absorption coefficients of both layers can be determined from the surface emission, the absorption of the bottom layer being obtained from the emission profile at large r, and that of the top layer being obtained from the emission profile close to the point where photons are injected.

A simple heuristic interpretation of these results is that photons reemitted close to their insertion point mostly travel in the upper layer, whereas those reemitted far from the insertion point mostly move within the bottom layer. Indeed, the large absorption coefficient of the top layer makes it very unlikely that any photons that travel for significant distances in that region will survive. The fact that the initial slope persists to ever greater r when the upper layer becomes increasingly thick is consistent with this interpretation. In Fig. 2(c) we plot the function $[\log(rG_r) + r(6\mu_2)^{1/2}]$ vs r. The line marked ∞ now has as its slope $(6\mu_2)^{1/2} - (6\mu_1)^{1/2}$. The regular spacing noted between the horizontal lines suggests that with proper calibration it may be possible to infer the thickness of the upper layer from the surface emission data.

2. *Absorption as a Function of Depth*

Similar features are seen in the curves for $A(z)$, which we designate here as the absorption at depth z. In Fig. 3(a) we show the absorption as a function of depth, and in Fig. 3(b) we plot the quantity $\{\log[A(z)] + z(6\mu_2)^{1/2}\}$. In accordance with analytical predictions[1] the diffential absorption in each region, far from the interface, is proportional to $\exp[-z(6\mu_i)^{1/2}]$, where μ_i is the absorption coefficient at the ith level. Figure 3(b)

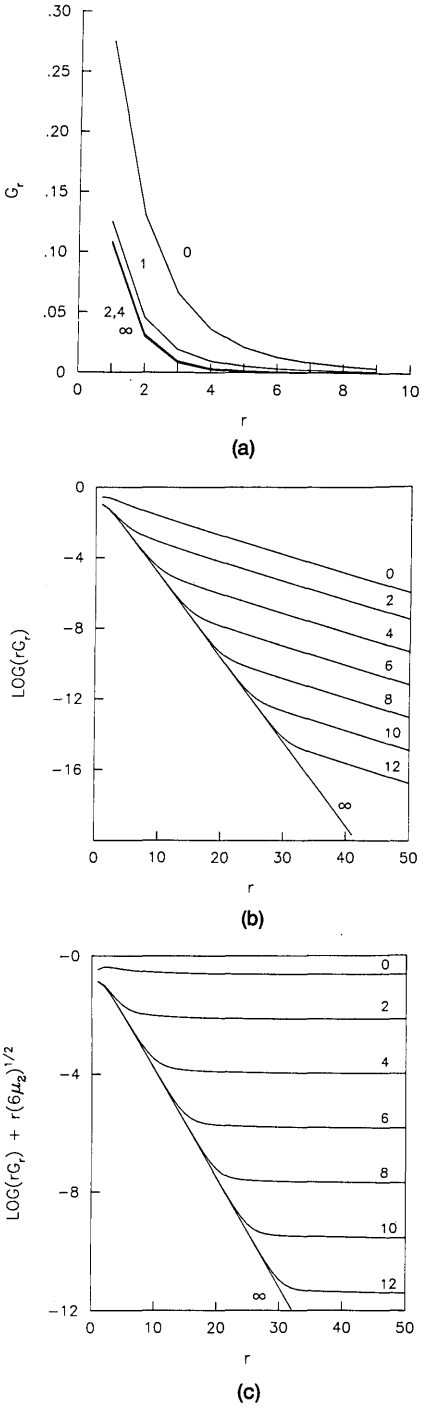

Fig. 2. Surface emission profiles as a function of distance from point of photon insertion for various values of top layer thickness $\mathcal{L}$. The absorption coefficient of the top layer is much greater than that of the bottom, namely, $\mu_1 = 0.2, \mu_2 = 0.01$: (a) the intensity in the rth ring G_r vs r; (b) $\log rG_r$ vs r; (c) $[\log rG_r + r(6\mu_2)^{1/2}]$ vs r (skewed values, see text). Note that distinguishing features appear only in the tails of the emission profiles, where the intensity has fallen off by several decades.

shows that the flux which enters the lower layer has been depleted exponentially by a factor that depends on the thickness of the upper layer.

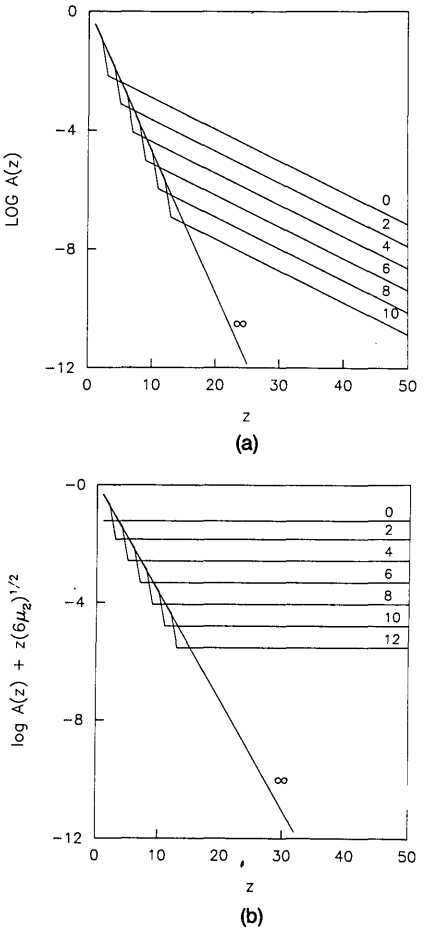

Fig. 3. Absorption as a function of depth for the same conditions as in Fig. 2: (a) $\log A(z)$ vs z; (b) $[\log A(z) + z(6\mu_2)^{1/2}]$ (skewed values).

3. *Average Path Length in the Medium*

We also have calculated the average total path length traversed by a photon that emerges within the rth ring. This quantity is of general interest when interpreting optical signals obtained from remote sensing measurements. In such cases the probability of photon interaction depends on the total path length over which photon migration occurs within the tissue. For example, knowledge of the mean path length is required for absolute measurement of microvascular blood flow and blood volume by laser Doppler techniques.[2]

When the medium through which the photons migrate is homogeneous, the average total path length, given that a photon is emitted at distance ρ from the point of injection, varies linearly with ρ as[1] $\langle n|\rho\rangle = 2 + 3\rho/(6\mu)^{1/2}$. Such behavior is indicated in Fig. 4(a) by the line designated as ∞, where we show results of calculations of $\langle n|r\rangle$ for a uniform medium having the absorption of the upper layer (approximating thereby a homogeneous semi-infinite medium). The other curves in that figure correspond to photons moving in a medium containing an upper region of finite thickness layered on top of a semi-infinite medium of lower

absorption. Again, the interpretation of the figure is that photons emerging close to the point of insertion mostly travel in the upper region. To be detected at a surface point far from the point of insertion, a photon has to travel within the lower region, as otherwise it tends to be absorbed. Indeed, for very large values of r, the average cumulative path length closely approximates that for photons which travel entirely in a medium having the properties of the bottom layer. This is indicated by the fact that the slope of the asymptotic curve marked 0 in Fig. 4(a) is given as $3/(6\mu_2)^{1/2}$.

An interesting representation of these data is achieved by dividing the curves $\langle n|r\rangle$, pertaining to different $\mathcal{L}$, by the corresponding values of the curve $\langle n|r\rangle_\infty$ for a homogeneous semi-infinite medium having the absorptive properties of the upper layer. In Fig. 4(b) we show the data of Fig. 4(a) plotted in this way. The curves seem to be evenly spread along the r axis for $\mathcal{L} \geq 2$ and spaced in proportion to $\mathcal{L}$. If the curves are shifted along the r axis, they overlap. Accordingly, if the curves of Fig. 4(b) are scaled along the abscissa by the factor $r/\mathcal{L}$, the midpoints coincide, although the curves do not otherwise superimpose.

4. *Average Depth of an Emitted Photon*

Another quantity that we are interested in—needed to determine which region of tissue is probed in remote sensing applications—is the average depth $\langle z|r\rangle$ at which a photon travels before surfacing within ring r. Results (still for the situation $\mu_1 = 0.2$, $\mu_2 = 0.01$) are shown in Fig. 5. Again, for photons emitted at small values of r, the average depth of penetration is almost identical to that of a lattice of infinite thickness. The transition noted in the curve at larger r indicates that photon migration occurs within the lower layer. As shown in Fig. 5, photons reemitted at larger r probe ever deeper regions of the tissue as the surface layer is thickened. The even spacing between the curves marked $\mathcal{L} = 2$, $\mathcal{L} = 4$, $\mathcal{L} = 6$, etc., indicates that, whatever the thickness of the upper layer, the lower layer is probed to nearly the same depth below its boundary with the upper layer. Due to the high absorption coefficient of the upper layer, the photons that surface are predominantly those which pass directly through the upper layer to the lower layer, where migration without absorption is more likely.

An ancillary point which now can be established is that, in a homogeneous medium, $\langle z|r\rangle$ seems to vary as r^α for sufficiently large r. The coefficient α is given approximately as $\alpha \doteq 0.5$. (Actually, present calculations indicate $\alpha = 0.54$ for $\mu = 0.01$, $\alpha = 0.50$ for $\mu = 0.2$, and $0.50 < \alpha < 0.54$ for $0.01 < \mu < 0.2$ with a tendency toward $\alpha = \frac{1}{2}$ as μ increases.) We recently found that, in a single-layer medium, the correct value of α indeed is 0.5.[10]

5. *Case $\mu_1 \ll \mu_2$*

We now examine what happens when the absorption of the top layer is much weaker than that of the bottom ($\mu_1 \ll \mu_2$). Let us consider as an example the inverse of the situation examined above, i.e., now assume $\mu_1 = 0.01$, $\mu_2 = 0.20$. Surface emission profiles for this case are shown in Fig. 6. In accordance with our intuition, the profiles corresponding to a surface layer of vanishing thickness decay more rapidly, as a function of r, than those for a medium with an overlaying region of

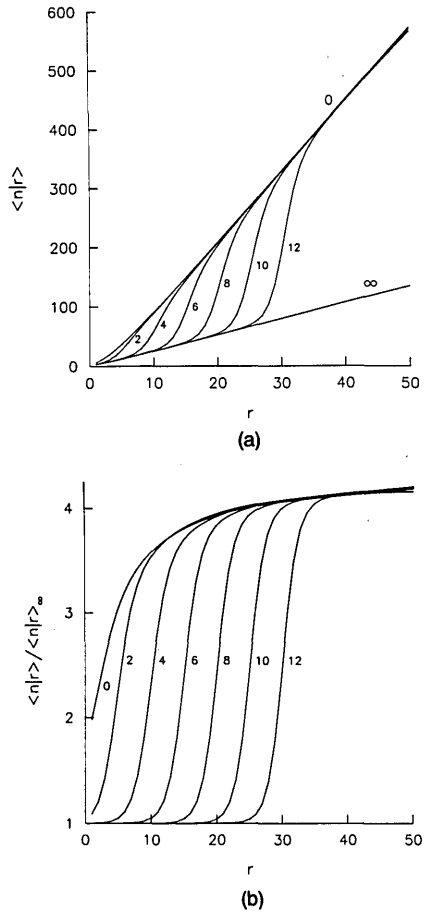

Fig. 4. Expected path length $\langle n|r\rangle$, given that a photon emerges at a point separated by r scattering lengths from the point of incidence: (a) $\langle n|r\rangle$ vs r; (b) normalized values, $\langle n|r\rangle/\langle n|r\rangle_\infty$ vs r, where $\langle n|r\rangle_\infty$ are values expected when $\mathcal{L} \to \infty$ (a homogeneous semi-infinite medium with the absorptive properties of the top layer). Conditions are identical to those stated in the caption of Fig. 2.

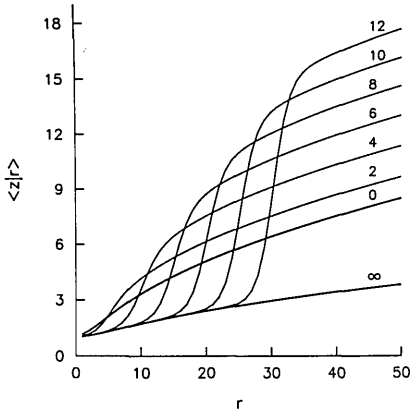

Fig. 5. Expected value of the depth $\langle z|r\rangle$ probed by photons emerging at r. Conditions are as described in Fig. 2 caption.

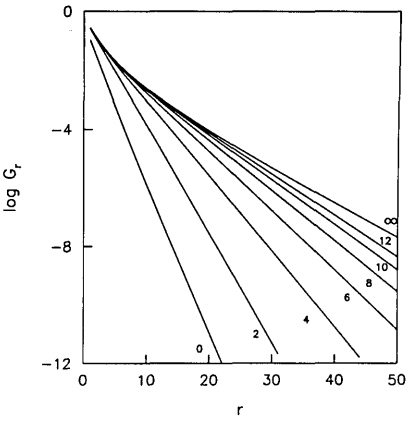

Fig. 6. LogG_r vs r. The top layer absorption coefficient here is much smaller than that of the lower region ($\mu_1 = 0.01$, $\mu_2 = 0.2$).

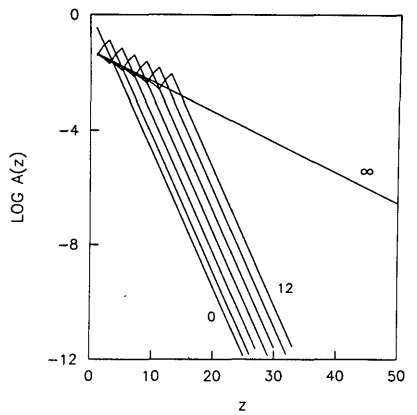

Fig. 7. Absorption profiles, log$A(z)$, vs z for the same conditions as shown in Fig. 6.

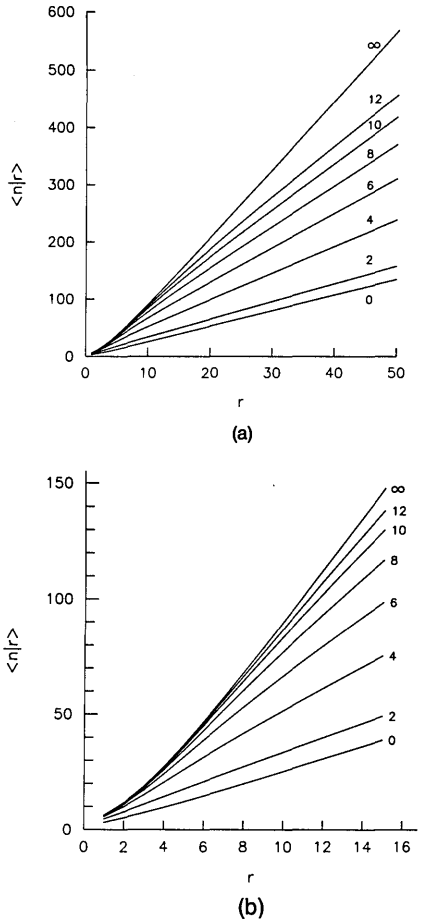

Fig. 8. (a) Expected path length, $\langle n|r\rangle$ vs r. Conditions identical to those of Fig. 6. (b) Same as (a), except the abscissa is expanded.

low absorption. However, it is somewhat surprising that, in contrast with the results in Fig. 2, the slope associated with the large r decay seems to change continuously with layer thickness $\mathcal{L}$. Thus it would be difficult to extract information about the two regions unless, perhaps, the absorbance of one of the regions were known. Additionally, we note the absence of any sharply delineated breakpoints in logG_r from which the thickness of the top layer can be ascertained. If properly calibrated, however, the slope of the large r decay might provide such information.

The absorption profiles, determined as a function of depth, also lack surprising features. In Fig. 7 we show log$A(z)$ vs z and note that the curves corresponding to different $\mathcal{L}$ are parallel, being displaced from one another by a factor proportional to the thickness of the upper, low absorbance, layer. The only unusual feature occurs at the boundary between the two layers, where a discontinuity in the number of absorbed photons is observed. This attribute reflects the fact that the number of absorbed photons is proportional to both the absorption coefficient and the flux; although the flux at the boundary is continuous, the absorption coefficients are discontinuous and cause a jump in an absorption profile. However, other than this, the curves shown in Fig. 7 have a simple interpretation, namely, that the top layer acts as a low absorption screen that decreases the flux arriving at the top of the lower layer, whence normal absorption subsequently occurs. In other words, the absorption in the lower layer can be estimated simply by decreasing the flux by an exponential factor whose argument is proportional to the product of the absorbance and the thickness of the upper layer.

The expected number of steps in a migration path $\langle n|r\rangle$ given that a photon is reemitted at r and the average depth probed by those photons $\langle z|r\rangle$ similarly lack any dramatic characteristics. In Fig. 8(a) we show $\langle n|r\rangle$. Note that the slopes of the curves at large r lie between the limiting values given by results for uniform media of either high or low absorbance, the value for the layered media changing continuously with layer thickness. However, the behavior for small r [Fig. 8(b)] indicates that, if the top layer is sufficiently thick, the average number of lattice collisions experienced by reemitted photons is approximately that of photons moving in material of uniform low absorbance, provided that $r \leq 0.6\mathcal{L}$. In Fig. 9 we show $\langle z|r\rangle$. The seemingly anomalous position of the curve for $\mathcal{L} = 0$ (corresponding to a homogeneous medium with $\mu = \mu_2$) reflects the fact that reemitted photons mostly

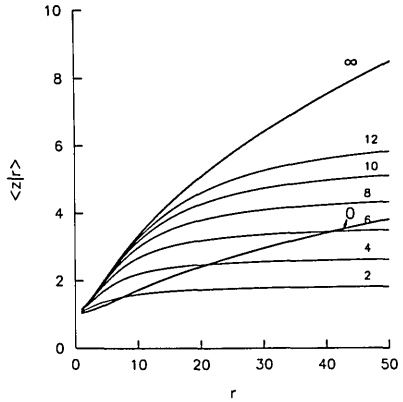

Fig. 9. Expected depth, $\langle z|r\rangle$ vs r. Conditions identical to those of Fig. 6.

move in the upper layer if the absorbance of that layer is much lower than that of the base. Although photons seemingly probe deeper into a uniform medium of high absorbance, fewer will escape from the surface.

Before concluding this section we remark that, by setting the absorbance of the bottom layer to a very large value, it is possible to mimic a thin tissue where the photons that pass through the upper layer are lost forever. This condition is approached, for example, in photoradiation treatment of metastatic ovarian cancer cells lying on top of highly absorbing spleen or liver tissue. An analogous situation arises when the underlying layer has a very long characteristic scattering length (as in free space). In this case, even if absorption is negligible, the lower layer cannot efficiently reflect photons back into the upper layer. Illumination of the wall of an inflated bladder within the peritoneal cavity might be modeled in this manner.

B. Layers of Similar Absorbance

1. *Surface Emission Profiles*

In almost all biological tissues, differences in absorption of different layers are due to small variations in the concentrations of ubiquitous chromophores. Thus the absorptions of different layers usually are similar, even if the tissue shows visible heterogeneity. For example, the marked yellow color of fatty atheroma, compared to a normal artery, results from only an approximately twofold difference in blue light absorption coefficients.[11] Another example where adjacent tissues might have slight, but discernible, differences in absorption is one in which tumors are present. Indeed, the detection of underlying tumors might be possible because of an increase in absorption arising from the hemoglobin in blood within such highly vascularized and hemorrhagic tissues.

In Fig. 10 we show the emission profiles $\log G_r$ for the cases (a) $\mu_1 = 0.1$, $\mu_2 = 0.05$ and (b) $\mu_1 = 0.05$, $\mu_2 = 0.1$. These values are typical of those for real biological tissues.[11–13] We infer from the computed data that it may be very difficult to discern the presence of a heterogeneous structure by cursory examination of the

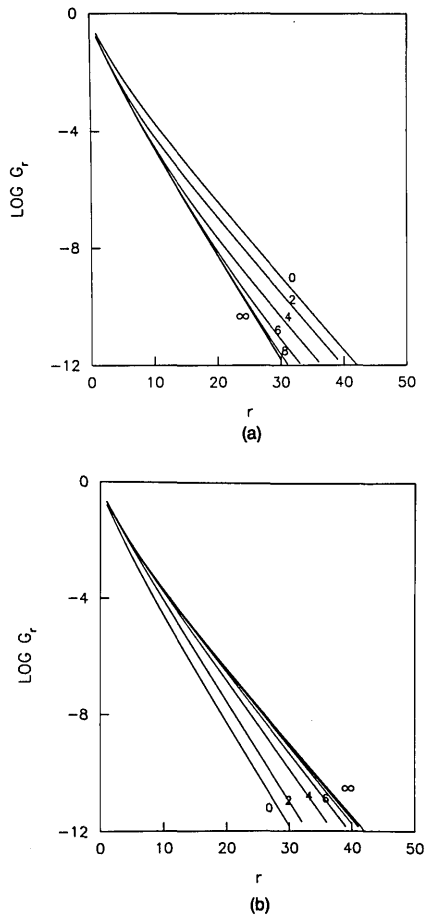

Fig. 10. Surface emission profiles, $\log G_r$ vs r, for media with layers having similar absorbance: (a) $\mu_1 = 0.1$, $\mu_2 = 0.05$; (b) $\mu_1 = 0.05$, $\mu_2 = 0.1$.

gross features of the emission profile. Yet some success might be realized in this regard if the absorbance of the top layer is greater than that of the bottom. In such cases [see Fig. 19(a)], sharp changes in slope should be observable in the curves of $\log G_r$ if data can be acquired at sufficiently large r. The presence of such sharp breaks will be a general characteristic of overlying layers of higher absorbance, provided that the data are free of noise. Similar features are seen in Fig. 2(a) ($\mu_1 = 0.2$, $\mu_2 = 0.01$), but, in that case of disparate absorptions, they are much more prominent. Also, as noted before in Fig. 6, when the top layer is less absorbing, the surface emission profiles seem to be smoother [see Fig. 10(b)]. The absorption profiles $A(z)$ and the curves of average migration (path) length $\langle n|r\rangle$ also have the same general appearance as those for the disparate layers case, except that the distinguishing features are less evident.

2. *Average Depth of an Emitted Photon*

In Fig. 11 we present results of calculations of the average depth $\langle z|r\rangle$, conditional on photon reemission within the rth ring. We again observe that the presence of a more highly absorbing layer strongly affects the depth probed by the photons that are reemitted at

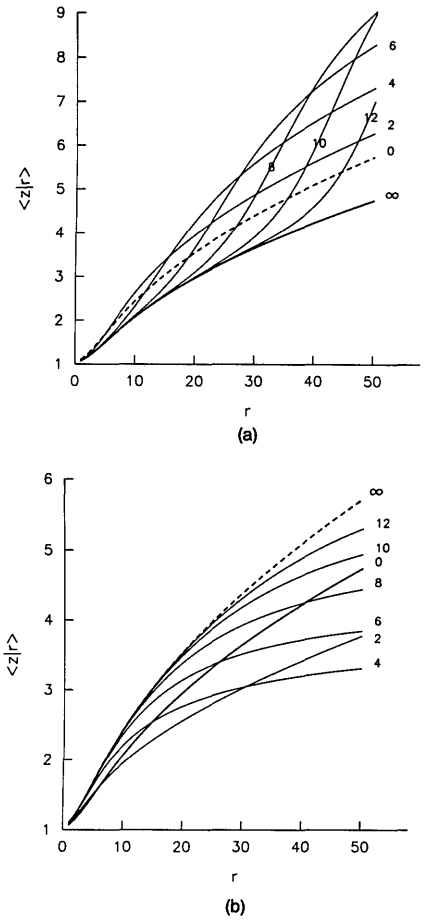

Fig. 11. Average depth $\langle z|r\rangle$ probed by emergent photons. Conditions are the same as in Figs. 10(a) and (b). The thick solid lines correspond to the situation where the entire medium has absorption $\mu = 0.1$; dotted lines correspond to the situation where the entire medium has absorption $\mu = 0.05$.

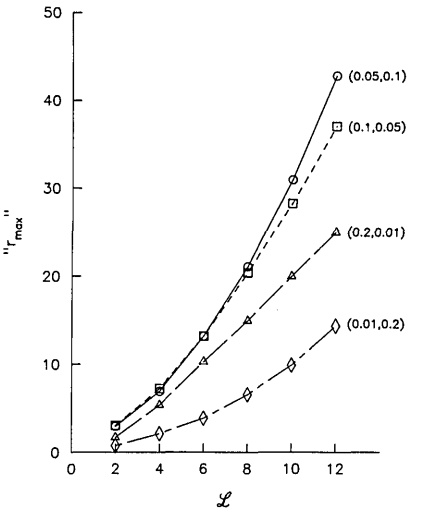

Fig. 12. Maximum distance along the surface for which emergent photons primarily probe the upper layer r_{max} as a function of $\mathcal{L}$. Numbers in parentheses are the values (μ_1,μ_2) corresponding to each curve. Data are determined by extrapolations of curves of $\langle z|r\rangle$, such as given in Fig. 11, to the point where $\langle z|r\rangle = (1 \pm 0.05)\langle z|r\rangle_\infty$.

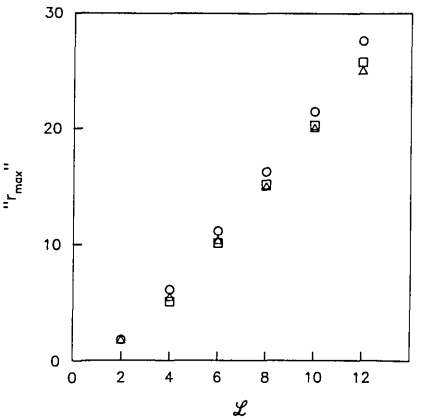

Fig. 13. r_{max} vs $\mathcal{L}$. Data obtained from extrapolations of surface emission curves, $\log G_r$, ●, and curves of $[\langle n|r\rangle/\langle n|r\rangle_\infty - 1]$, ■, compared with data for $\langle z|r\rangle$ shown in Fig. 12, ▲.

larger r (see Figs. 5 and 9). The thick solid lines in Figs. 11 correspond to a situation where the entire medium is composed of the more highly absorbing material, and the dotted lines correspond to a uniform medium of lower absorbance. By comparing the results shown in Fig. 11(a) with those in Fig. 11(b), we note that if the higher absorbance material underlies the lower ($\mu_1 < \mu_2$), the average depth probed by reemitted photons is less than that which would occur in a homogeneous medium consisting of the material of the top layer. In contrast, if the higher absorbance material constitutes the surface layer ($\mu_1 > \mu_2$), the depth that is probed increases by an amount proportional to the thickness of the upper layer. For photons detected at sufficiently large r, the additional depth is approximately equal to a fraction of the surface layer, where the fraction varies from 0 to 1 as μ_1/μ_2 varies from 1 to a large value.

Of course, essentially only the properties of the top layer are probed if the reemitted photons are detected close to the point of insertion. A rough estimate of the maximum value of r at which the reemitted photons primarily probe the surface can be obtained from Fig. 11 by extrapolating to the points where the curves for finite layer thickness superimpose on the curve for infinite thickness. Results are shown in Fig. 12, not only for the cases considered above but also for several other combinations of absorption coefficients. These estimates of r_{max} are consistent with estimates obtained from other quantities that we have calculated. For example, in Fig. 13 we show (for $\mu_1 = 0.2$, $\mu_2 = 0.01$) the values of r_{max} obtained by determining where the surface emission profiles differ by 5% (i.e., $\log G(r|\mathcal{L})/G(r|\mathcal{L} = \infty) = \log 1.05 = 0.0212$). The values are close to those given in Fig. 12 and agree also with estimates of r_{max} obtained by setting $|\langle n|r\rangle/\langle n|r\rangle_\infty - 1| = 0.05$ [see Figs. 2(b) and 4(b)].

IV. Remarks

The methodology of exact enumeration provides a means to test accurately, with greater precision than

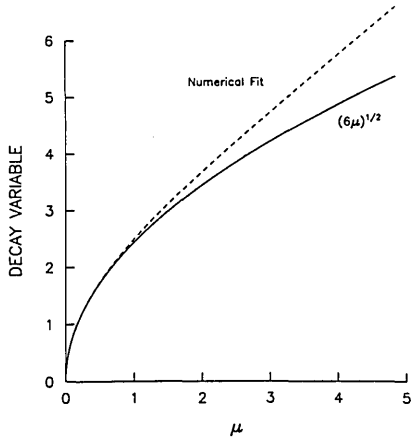

Fig. 14. Comparison between theoretical value of decay rate of $A(z)$ in homogeneous media $(6\mu m)^{1/2}$, as given by the theory developed in Ref. 1, and the rate obtained from direct enumeration of probability densities, as described in Sec. II. Solid line, theoretical value; dotted line, numerical computation.

by our earlier Monte Carlo simulations,[1] several of the mathematical expressions that we previously derived. For the most part, our earlier analytical work has been substantiated. However, an interesting point that now seems to be established by these calculations, particularly results shown in Figs. 5, 9, and 11, is that the power law dependence of $\langle z|r\rangle$ on r is given as $\langle z|r\rangle \sim r^{1/2}$.[10] Another mathematical point that can be clarified is whether the depth profile for homogeneous absorption $A(z)$ truly is given by the expression $A(z) \sim \exp[-z(6\mu)^{1/2}]$, even if the absorption coefficient μ is very large. In the latter case the flux would decrease rapidly near the surface, and the mixing of lattice and continuum models, as done in Ref. 1, might not be appropriate. Indeed, as shown in Fig. 14, when μ exceeds a value of $\sim$3, the errors in the decay rate exceed 10%.

As pointed out in Sec. I, we have ignored anisotropic scattering. We previously argued[1] that the artifice of isotropic scattering, such as is used here, is equivalent to redefining the mean scattering length. By asserting that the scattering angle distribution is uniform, we implicitly set the scattering length to be the rms distance (number of steps) that a photon travels before it turns on average through an angle of 90° with respect to its incident direction. We have performed a limited number of Monte Carlo simulations for homogeneous media whose scattering is spatially anisotropic and indeed have found that the results can be scaled to mimic those of isotropic media.[10] If necessary, the computational scheme used here could be extended to account for unequal scattering angle probabilities by increasing the size of probability density matrices to provide a memory of preceding steps. Another factor not accounted for is the possible difference in scattering length in the different layers. This too presumably could be taken into account by modifying the transition matrices for probability densities.

Our present results indicate that, when an underlying tissue layer has a lower absorption than the upper layer, photons reemitted sufficiently far from the point of insertion most likely will have moved primarily within the underlying layer. Thus the optical characteristics of the lower tissue layer can be evaluated by examining surface emission at values of ρ greater than $\mathcal{L}$, where $\mathcal{L}$ is the thickness of the superficial layer. Unless obscured by noise, a discontinuity in the diffuse surface emission will be observed, and the optical properties of the lower layer can be ascertained with good precision. In contrast, when the lower layer is more highly absorbing than the superficial layer, the uncovering of detailed information about the lower layer is more problematic. In this case the discontinuity in tissue properties causes an increased loss of deeper photon trajectories, and photons that emerge at larger ρ predominantly sample the interface between the two layers. Consequently, the reemission profile at large ρ depends in a complicated way on optical characteristics of both homogeneous layers, with the consequence that the optical identity of the lower layer may remain ambiguous.

In both cases, one might have to measure emission profiles in a region of ρ where the intensities are very weak compared with those near the point of photon insertion. Alternatively, by using multiple wavelengths for which the absorption coefficients vary in different fashions, it might be possible to discern differences in the emission profiles at smaller ρ that contain significant information. In either case it might be necessary to design special instrumentation to achieve the necessary range and sensitivity, but, as suggested by these calculations, such an effort could be very rewarding. Concomitant theoretical analysis is required, however, whenever remote sensing of biological tissue is undertaken in which the mean depth sampled is greater than the thickness of a homogeneous layer.

S. Havlin gratefully acknowledges support from the USA-Israel Binational Science Foundation.

References

1. R. Bonner, R. Nossal, S. Havlin, and G. H. Weiss, "Model for Photon Migration in Turbid Biological Media," J. Opt. Soc. Am. A **4**, 423 (1987).
2. R. Bonner and R. Nossal, "Model for Laser Doppler Measurements of Blood Flow in Tissue," Appl. Opt. **20**, 2097 (1981).
3. R. F. Bonner, T. R. Clem, P. D. Bowen, and R. L. Bowman, "Laser Doppler Real-Time Monitor of Pulsatile and Mean Blood Flow in Tissue Microcirculation," in *Scattering Techniques Applied to Supramolecular and Nonequilibrium Systems*, S-H. Chen, B. Chu, and R. Nossal, Eds. (Plenum, New York, 1981).
4. G. H. Weiss and R. J. Rubin, "Random Walks, Theory, and Selected Applications," Adv. Chem. Phys. **52**, 363 (1983).
5. W. E. Blumberg, "Light Propagation in Human Tissues," Biophys. J. **51**, No. 2, Part 2), 288a (1987).
6. D. R. Dorion, L. O. Svaasand, and A. E. Profio, "Light Dosimetry in Tissue, Application to Photoradiation Therapy," in *Porphyrin Photosensitization*, D. Kessel and T. J. Dougherty, Eds. (Plenum, New York, 1983).
7. C. Kittrell, R. L. Willett, C. Santos-Pacheo, N. B. Ratliff, J. R. Kramer, E. G. Malk, and M. S. Feld, "Diagnosis of Fibrous

Arterial Atherosclerosis Using Fluorescence," Appl. Opt. **24**, 2280 (1985).
8. D. Ben-Avraham and S. Havlin, "Diffusion of Percolation Clusters at Criticality," J. Phys. A **15**, L691 (1982); S. Havlin and D. Ben-Avraham, "Diffusion in Disordered Media," Adv. Phys. **36**, 695 (1987).
9. S. Havlin, G. H. Weiss, J. E. Kiefer, and M. Dishon, "Exact Enumeration of Random Walks with Traps," J. Phys. A **17**, L347 (1984).
10. G. H. Weiss, R. Nossal, and R. J. Bonner, "Statistics of Penetration Depth of Photons Re-Emitted from Irradiated Tissue," Mod. Optics (in press).
11. M. R. Prince, T. F. Deutsch, M. M. Mathews-Roth, R. Margolis, J. A. Parrish, and A. R. Oseroff, "Preferential Light Absorption in Atheromas *in vitro*," J. Clin Invest. **78**, 295 (1986).
12. P. J. Kolari, "Penetration of Unfocused Laser Light into the Skin," Arch. Dermatol. Res. **277**, 342 (1985).
13. B. C. Wilson and M. S. Patterson, "The Physics of Photodynamic Therapy," Phys. Med. Biol. **31**, 327 (1986).

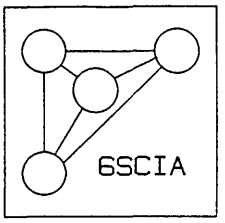

IAPR

THE 6TH SCANDINAVIAN CONFERENCE ON IMAGE ANALYSIS

FIRST ANNOUNCEMENT

The 6th Scandinavian Conference on Image Analysis (6SCIA) will be arranged by the Pattern Recognition Society of Finland from June 19 to June 22, 1989. The conference is sponsored by the International Association for Pattern Recognition. The conference will be held at the University of Oulu. Oulu is the major industrial city in North Finland, situated not far from the Arctic Circle.

PROGRAM

The program will consist of invited papers and contributed papers on

- computer vision
- image processing
- pattern recognition
- perception
- parallel algorithms and architectures
- applications

The official language of the Conference is English.

SUBMISSION OF PAPERS

Authors are invited to submit four copies of an extended summary of at least 1000 words of each of their papers to:

Matti Pietikäinen
6SCIA Program Chairman
Dept. of Electrical Engineering
University of Oulu
SF-90570 OULU, Finland

tel. + 358-81-352765
fax + 358-81-561278
telex 32 375 oylin sf
net scia@steks.oulu.fi

The summary should contain sufficient detail, including a clear description of the salient concepts and novel features of the work. Deadline for submission of summaries is December 1, 1988. Authors will be notified of acceptance by January 31, 1989 and final camera-ready papers will be required by March 31, 1989.

EXHIBITION

An exhibition is planned. Companies and institutions involved in image analysis and related fields are invited to exhibit their products on posters, video or in demonstration stands. Please indicate your interest to take part by contacting the Program Chairman.

SOCIAL PROGRAM

A social program will be arranged, including possibilities to enjoy the location of the conference, the sea and the midnight-sun. There are excellent possibilities to make post-conference tours e.g. to Lapland or to the lake district of Finland.

CONFERENCE COMMITTEE

Erkki Oja, Conference Chairman
Matti Pietikäinen, Program Chairman
Juha Röning, Chairman local organization
Hannu Hakalahti, Chairman exhibition
Jan-Olof Eklundh, Sweden
Stein Grinaker, Norway
Teuvo Kohonen, Finland
L.F. Pau, Denmark